



Mn/TiO₂ and Mn–Fe/TiO₂ catalysts synthesized by deposition precipitation—promising for selective catalytic reduction of NO with NH₃ at low temperatures

Siva Sankar Reddy Putluru ^a, Leonhard Schill ^{a,b}, Anker Degn Jensen ^b, Bernard Siret ^c, Franck Tabaries ^c, Rasmus Fehrman ^{a,*}

^a Centre for Catalysis and Sustainable Chemistry, Department of Chemistry, Building 207, Technical University of Denmark, DK-2800 Kgs. Lyngby, Denmark

^b Combustion and Harmful Emission Control Research Centre, Department of Chemical and Biochemical Engineering, Building 229,

Technical University of Denmark, DK-2800 Kgs. Lyngby, Denmark

^c LAB SA, 259 Avenue Jean Jaurès, 69364 Lyon Cedex 07, France

ARTICLE INFO

Article history:

Received 1 September 2014

Received in revised form 15 October 2014

Accepted 22 October 2014

Available online 1 November 2014

Keywords:

SCR of NO with NH₃

Mn–Fe/TiO₂

Deposition precipitation.

ABSTRACT

Mn/TiO₂ and Mn–Fe/TiO₂ catalysts have been prepared by impregnation (IMP) and deposition-precipitation (DP) techniques and characterized by N₂ physisorption, XRPD, NH₃-TPD, H₂-TPR, XPS and TGA. 25 wt% Mn_{0.75}Fe_{0.25}Ti-DP catalyst, prepared by deposition precipitation with ammonium carbamate (AC) as a precipitating agent, showed superior low-temperature SCR (selective catalytic reduction) of NO with NH₃. The superior catalytic activity of the 25 wt% Mn_{0.75}Fe_{0.25}Ti-DP catalyst is probably due to the presence of amorphous phases of manganese oxide, iron oxide, high surface area, high total acidity, acid strength and ease of reduction of manganese oxide and iron oxide on TiO₂ in addition to formation of an SCR active MnO_x phase with high content of chemisorbed oxygen (O_α). The optimum catalyst might be used as tail-end SCR catalysts in, e.g., biomass-fired power plants and waste incineration plants.

© 2014 Elsevier B.V. All rights reserved.

1. Introduction

The selective catalytic reduction (SCR) of NO with NH₃ is widely employed for control of NO_x emissions from stationary sources. The most common commercially used catalyst is vanadia well dispersed on a titania support promoted by tungsten oxide (V₂O₅–WO₃/TiO₂) [1–3]. The commercial catalyst has high activity and selectivity in SCR of NO with NH₃ at 300–400 °C. To achieve this temperature, the commercial catalysts are placed in high dust positions in the flue gas stream [4]. However, high content of ash with impurities (like K₂O, CaO and As₂O₃) and SO₂ in the flue gas reduces the catalyst performance and it is deactivated over time [5,6]. Therefore a tail-end and at low dust, downstream of the flue gas desulphurization unit is attractive. At the tail-end configuration, the lower temperature and levels of SO₂ in the flue gas allow the use of more active catalyst formulations, mainly because the oxidation of SO₂ to SO₃ is not as severe. At the same time, the life of the catalyst also increases because of decreased erosion and fouling at the low dust level [7]. However, tail-end configuration demands a catalyst which is much more active at these low temperatures (i.e. 140–200 °C) than the

V₂O₅–WO₃/TiO₂ catalyst in order to avoid expensive reheating of the flue gas to around 350 °C.

Over the last decade, there has been great interest in the development of low-temperature SCR catalysts containing transition metal oxide catalysts like V₂O₅/TiO₂, Fe₂O₃/TiO₂, CuO/TiO₂ and MnO_x/TiO₂ [8–12]. Among them, Mn-containing catalysts have shown excellent low-temperature performance [13,14]. Furthermore, it has been revealed that bimetallic Mn catalysts are more active and selective. Thus, highly active bimetallic low-temperature SCR catalysts reported in the literature are Mn–Fe/TiO₂ [14–16], MnO_x–CeO₂ [17], Mn–Ni/TiO₂ [14,18,19] and Mn–Cu/TiO₂ [14,15,18]. Among the bimetallic catalysts, the effect of adding transition metals to Mn/TiO₂ is significant. Especially, Fe enhances the low-temperature SCR activity, by better dispersion on TiO₂ and retardation of sintering [13,14,16].

The low-temperature SCR activity of MnO_x catalysts depends on the preparation method, Mn precursor, Mn loading, crystallinity and oxidation state of MnO_x. Jiang et al. [20] prepared Mn/Ti catalysts by the three most common synthesis methods (sol-gel, impregnation and coprecipitation). The sol-gel method prepared catalyst showed the highest activity with an optimum catalyst composition of Mn/Ti (mol/mol) of 0.4. Strong metal–support interactions, large surface area, high concentrations of hydroxyl groups and amorphous Mn on the surface of TiO₂ are the reasons for

* Corresponding author. Tel.: +45 45252389; fax: +45 45883136.

E-mail address: rf@kemi.dtu.dk (R. Fehrman).

excellent SCR performance of the sol-gel-prepared Mn/Ti catalyst [20]. Li et al. [21] studied the effect of TiO₂-supported Mn precursors (acetate and nitrate) on the catalytic activities of NO by ammonia. Manganese acetate as precursor led to a significantly higher activity, especially in the low-temperature region. Roy et al. [15] reported that Ti_{0.9}Mn_{0.05}Fe_{0.05}O_{2-δ} (10 wt% metal) catalysts prepared by solution combustion exhibited high SCR activity and high N₂ selectivity over a wide temperature range.

Low-temperature Mn/TiO₂ catalysts are reported having an optimum loading of 20 wt% [13,18] while the optimum loading of Mn–Fe/TiO₂ catalysts is 10 wt% Mn–10 wt% Fe [16] synthesized by impregnation. Overall, the active metal content in low-temperature Mn/TiO₂ catalysts is high (about 20 wt% metal on TiO₂) compared to the conventional V₂O₅–WO₃/TiO₂ formulations (7–10 wt% metal on TiO₂). Unsupported manganese oxide catalysts in amorphous phase with high surface area also showed high SCR activity at low reaction temperatures [22,23]. It is reported that the most active oxide composition of Mn is MnO₂ [18,19,22,24] followed by Mn₅O₈, Mn₂O₃ and Mn₃O₄ [25].

In the present work, we studied the Mn/TiO₂ and Mn–Fe/TiO₂ catalysts prepared by deposition precipitation and impregnation regarding the activity for the SCR reaction with NH₃ as reducing agent. A comparison was also made with a 3 wt% V₂O₅–7 wt% WO₃/TiO₂ standard catalyst (VWTi) under identical conditions. All catalysts were characterized by various techniques.

2. Experimental

2.1. Catalyst preparation and characterization

Anatase TiO₂ DT-51 (Crystal Global with a sulfur content of ~1.25 wt%, surface area of 87 m²/g) was used as support material. The Mn/TiO₂ catalysts were prepared by two methods: impregnation and deposition precipitation. By the impregnation method (IMP), the required amount of manganese (II) acetate tetrahydrate ((CH₃COO)₂Mn·4H₂O, 99.9%, Aldrich) and 1 g of TiO₂ were added to 20 ml of deionized water. The slurry was exchanging for 1 h at room temperature and the excess water was then slowly evaporated with continuous stirring. The solid obtained was oven-dried at 120 °C for 12 h and then calcined in air at 400 °C for 2 h. The catalysts were designated as 5–30 wt% MnTi-IMP referring to wt% of Mn.

By deposition-precipitation (DP), the Mn/TiO₂ catalysts were prepared by slow addition of solutions of precipitating agents (urea (1 M), ammonium nitrate (1 M), ammonium hydroxide (20 vol.%) and ammonium carbamate (1 M), Aldrich). The water of the resulting slurry was slowly evaporated with continuous stirring followed by the same calcination procedure as that of the impregnated catalysts. The catalysts were designated as 1–20 wt% MnTi-DP. The bimetallic Mn–Fe catalysts were also prepared by the IMP and DP methods. Manganese (II) acetate tetrahydrate ((CH₃COO)₂Mn·4H₂O, 99.9%, Aldrich) and iron (III) nitrate nonahydrate (Fe(NO₃)₃·9H₂O, 99.9%, Aldrich) were used as precursors. The IMP and DP catalysts were designated as 20–40 wt% Mn_xFe_{1-x}Ti-IMP and 15–30 wt% Mn_xFe_{1-x}Ti-DP, respectively. Here x and 1-x represent molar fractions of Mn and Fe, respectively, e.g., 25Mn_{0.75}Fe_{0.25}Ti-DP. DP refers to the use of ammonium carbamate as the precipitating agent, unless otherwise stated.

X-ray powder diffraction (XRPD) were performed on a Huber G670 powder diffractometer using Cu K α radiation within a 2 θ range of 2–60° in the steps of 0.02°. The crystallite size was measured using the Debye–Scherrer equation. BET surface areas of the samples were determined from nitrogen physisorption measurements on about 100 mg sample at liquid nitrogen temperature with

a Micromeritics ASAP 2010 instrument. The samples were heated to 200 °C for 1 h prior to the measurement.

NH₃-TPD experiments were conducted on a Micromeritics Autochem-II instrument. In a typical TPD experiment, 100 mg of the dried sample was placed in a quartz tube and pretreated in flowing He at 100 °C for 1 h and the sample was then treated with anhydrous NH₃ gas (Air Liquide, 5% NH₃ in He). After NH₃ adsorption, the sample was flushed with He (50 ml/min) for 100 min at 100 °C. Finally, the TPD operation was carried out by heating the sample from 100 to 700 °C (10 °C/min) under a flow of He (50 ml/min).

H₂-TPR studies were also conducted on a Micromeritics Autochem-II instrument. In a typical experiment, 100 mg of the dried sample was placed in one arm of a U-shaped quartz tube on quartz wool. The TPR analysis was carried out in a reducing mixture (50 ml/min) consisting of 5% H₂ and balance Ar (Air Liquide) from 60 to 550 °C (10 °C/min). The hydrogen concentration in the effluent stream was monitored by a thermal conductivity detector (TCD) and the H₂ consumption values were calculated from calibration experiments.

TGA measurements were conducted on a Mettler Toledo TGA/DSC 1 SF instrument. About 25 mg of the sample was placed in a 70 μ L alumina crucible and heated from room temperature up to 600 °C with a heating rate of 10 °C/min under a N₂ flow of 20 mL/min.

XPS measurements were conducted on a Thermo scientific system at room temperature using Al K α radiation (1484.6 eV). Before acquisition of the data, the sample was outgassed for about 1 h in vacuum to minimize surface contamination. The XPS instrument was calibrated using Au as the standard. The spectra were deconvoluted using Thermo Scientific Avantage Data system software.

2.2. Catalytic activity measurements

The SCR activity measurements were carried out at atmospheric pressure in a fixed-bed reactor loaded with 50 mg of fractionized (180–300 μ m) catalyst at a flow rate of 300 mL min⁻¹. The inlet concentrations were: NO = 1000 ppm, NH₃ = 1000 ppm, O₂ = 4% and H₂O = 2.3% with He as balance gas. During the experiments, the temperature was increased in steps of 25 °C from 125 to 300 °C, while the NO and NH₃ concentrations were continuously monitored by a Thermo Electron Model 17C chemiluminescence NH₃–NO_x gas analyzer. The N₂O concentration was further measured by gas chromatography (Shimadzu 14 B GC, TCD detection, poraplot column). The activity was measured after attaining steady state and care was taken not to reach 100% conversion to keep the catalyst stressed and to allow calculation of rate constants.

The activity of the Mn and VWTi catalysts is given by NO conversion (%) and the relative rate constant ($k_{\text{Mn cat}}/k_{\text{VWTi}}$) to illustrate the activity of Mn catalysts compared to the standard catalyst. The first-order rate constants (cm³/g s) were obtained from the conversion of NO as [17]:

$$k = -\frac{F}{w} * \ln(1 - X)$$

where F denotes the flow rate (cm³/s), w the catalyst mass and X the fractional conversion of NO.

3. Results and discussion

Fig. 1 shows the NO conversion profiles of 5–30 wt% MnTi-IMP and VWTi catalysts as a function of reaction temperature. The MnTi-IMP catalysts exhibited significant NO conversion below 225 °C, while the conventional VWTi catalyst showed higher NO conversion at reaction temperatures above 250 °C. By gradual increase in Mn loading of the MnTi-IMP catalysts, the NO conversion increased until 20 wt%, and then

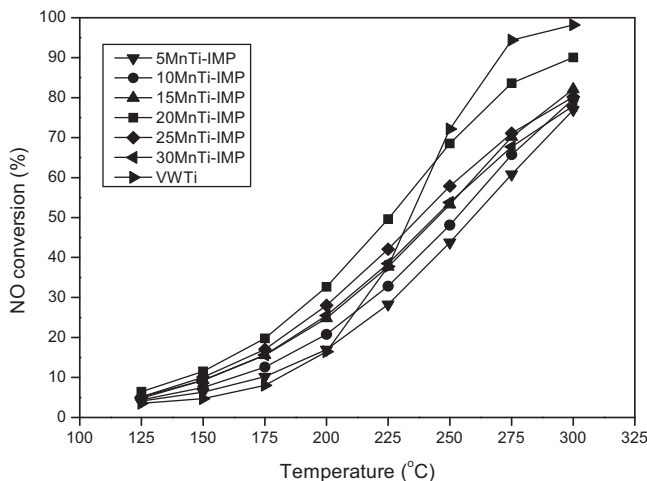


Fig. 1. Catalytic activity profiles of MnTi-IMP catalysts with different Mn loadings.

further increase of Mn loading lead to gradual decrease of the conversion. A similar loading effect was observed by Jiang [20] and Qi et al. [16] with an optimum metal loading of 19.4 and 20 wt%, respectively. The optimum 20MnTi-IMP and conventional VWTi catalysts exhibited NO conversions of 32.7 and 16.5% at 200 °C, respectively, illustrating the higher low-temperature SCR activity of Mn-based catalysts compared to the standard.

Fig. 2 shows the NO conversion profiles of 5 wt% Mn/TiO₂ catalysts prepared by deposition precipitation (DP) using various basic precipitating agents as a function of reaction temperature. The 5MnTi catalysts prepared by DP method exhibited increased NO conversion in the order: ammonium carbamate > urea > ammonium nitrate > ammonium hydroxide. Thus the 5 wt% Mn/TiO₂ catalyst prepared with ammonia carbamate, urea, ammonium nitrate and ammonium hydroxide precipitating agents exhibited NO conversion of 48.6, 22.3, 22.0 and 16.8% at 200 °C, respectively. Such a change in SCR activity with different precipitating agents could be due to anionic effect. Similar anionic effect was observed by Kang et al. [22] that carbonate as an anion showed higher NO_x conversion than those prepared with hydroxides. Therefore, Mn/TiO₂ catalysts were synthesized by deposition precipitation using ammonium carbamate as precipitating reagent for further optimization.

Fig. 3 shows the NO conversion profiles of 1–20 wt% MnTi-DP catalysts prepared by ammonium carbamate as precipitating

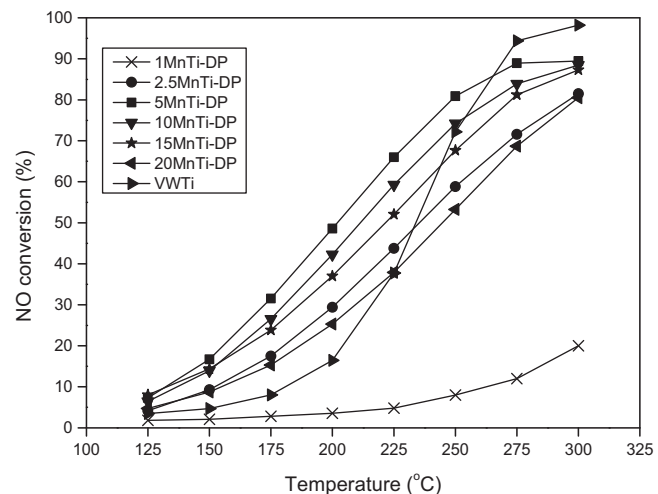


Fig. 3. Catalytic activity profiles of MnTi-DP catalysts with different Mn loadings prepared by ammonium carbamate as precipitant.

reagent vs the reaction temperature. The MnTi-DP catalysts exhibited superior low-temperature activity compared to the MnTi-IMP catalysts. The effect of Mn loading on MnTi-DP catalysts is similar to MnTi-IMP but the optimum Mn loading was found to be much lower, i.e. 5 wt%. Especially, 5MnTi-DP and 10MnTi-DP catalysts showed superior activity even at 250 °C when compared to conventional VWTi catalyst. Thus, by the DP method, enhanced activity, broad reaction temperature window and furthermore a substantial decrease in Mn loading can be achieved.

Transition metal-promoted Mn/TiO₂ catalysts, i.e. by metals like Fe, Cu and Ni, have shown good performance in low-temperature SCR with Fe giving the most favorable effect on the catalytic activity [13,14,16]. Transition metal-doped Mn/TiO₂ catalyst has high resistance to sintering, better Mn dispersion and enhanced active MnO₂ phase [13,14]. Further, the transition metal-promoted Mn/TiO₂ catalysts showed activity for NO oxidation to NO₂ at low temperatures [11,16]. We decided therefore to focus on Fe-promoted Mn/TiO₂ catalysts. Fig. 4 shows the NO conversion profiles of 20–40 Mn_{0.75}Fe_{0.25}Ti-IMP and 15–30 Mn_{0.75}Fe_{0.25}Ti-DP catalysts. All the Mn–Fe bimetallic catalysts showed superior SCR activity compared to the VWTi catalyst. Especially, the 35 Mn_{0.75}Fe_{0.25}Ti-IMP and 25 Mn_{0.75}Fe_{0.25}Ti-DP catalysts exhibited high SCR activity with NO conversions of 68.5 and 96.75%, respectively, at 200 °C. Presence of Fe increases the optimum total metal loading from 20 to 35 wt% for the IMP catalysts and from 5 to 25 wt% for the DP catalysts, indicating that Fe is promoting Mn dispersion.

Fig. 5 shows the SCR activity of 25 wt% MnFeTi-DP catalyst with different Mn–Fe mole fractions. The results show that the optimum SCR activity is obtained at a mole Mn fraction of 0.75. Especially the 25 Mn_{0.75}Fe_{0.25}Ti-DP catalyst, with the optimum Mn–Fe content, displayed superior low-temperature activity compared to the other catalysts. It should be mentioned that the 25 Mn_{0.75}Fe_{0.25}Ti-DP catalyst displayed 55 ppm of N₂O under wet conditions (2.3 vol.%), however, further increase in water (up to 10 vol.%) caused almost 0 ppm levels of N₂O at 200 °C. This shows that under industrial conditions N₂O emissions would not be an issue for this catalyst.

In Fig. 6, the optimum catalysts are compared with the VWTi catalyst by plotting the rate constant ratio ($k_{\text{MnFe}}/k_{\text{VWTi}}$) vs the reaction temperature. All the Mn-containing catalysts showed superior relative activity below 250 °C with a maximum around 175 °C. Thus, the 20MnTi-IMP, 5MnTi-DP, 35Mn_{0.75}Fe_{0.25}Ti-IMP and 25Mn_{0.75}Fe_{0.25}Ti-DP catalysts showed relative activities compared to the standard VWTi catalyst of 2.6, 4.5, 7.7 and 26.9, respectively, at 175 °C. The 20MnTi-IMP, 5MnTi-DP, 35Mn_{0.75}Fe_{0.25}Ti-IMP,

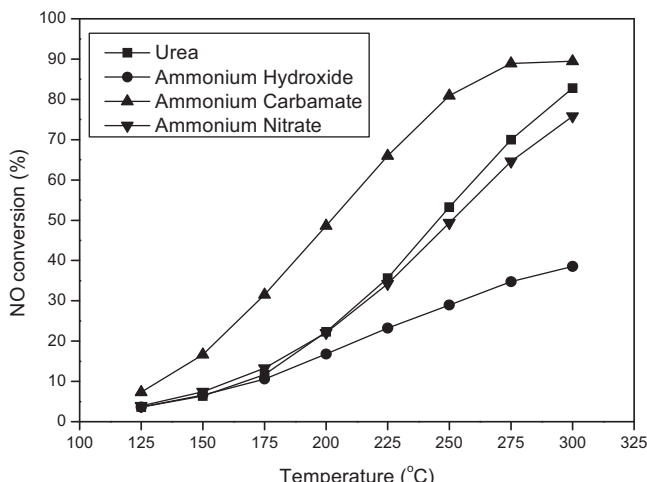


Fig. 2. Catalytic activity of 5MnTi catalysts prepared by different precipitants.

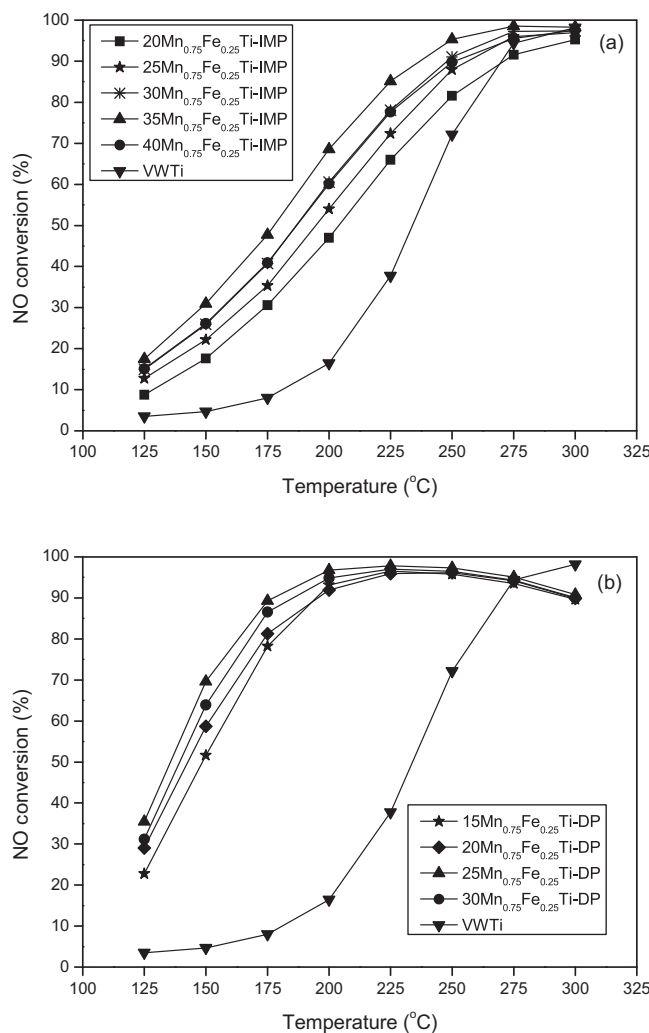


Fig. 4. Catalytic activity profiles of $Mn_{0.75}Fe_{0.25}Ti$ -IMP and $Mn_{0.75}Fe_{0.25}Ti$ -DP catalysts with different metal loadings.

$25Mn_{0.75}Fe_{0.25}Ti$ -DP and VWTi catalysts displayed rate constants of 21.7, 37.43, 64.0, 222.9 and $8.3\text{ cm}^3\text{ g}^{-1}\text{ s}^{-1}$, respectively, at 175°C . A comparison was reported by Yang et al. [26] on the most active low-temperature SCR formulations at 150°C without the presence of water in the feed. Among the supported catalysts, the most active was reported to be a 10%Fe–10%Mn/TiO₂ catalyst with a rate constant of $65.6\text{ cm}^3\text{ g}^{-1}\text{ s}^{-1}$ [16,26] followed by MnO_x –WO₃/γ-Al₂O₃ catalyst with a rate constant value of $21.5\text{ cm}^3\text{ g}^{-1}\text{ s}^{-1}$ [26,27]. Unsupported MnO_x –CeO₂ and $(Fe_{2.5}Mn_{0.5})_{1-\delta}O_4$ formulations displayed rate constants of 121 and $109\text{ cm}^3\text{ g}^{-1}\text{ s}^{-1}$, respectively [26].

Table 1
Physicochemical properties of Mn–Fe/TiO₂ catalysts.

Catalyst	Metal (wt.%) Mn	Fe	Surface area (m ² /g)	Acidity (μmol/g)
10MnTi-IMP	10	0	60	319
20MnTi-IMP	20	0	55	271
30MnTi-IMP	30	0	42	253
2.5MnTi-DP	2.5	0	81	393
5MnTi-DP	5	0	79	525
10MnTi-DP	10	0	77	371
20Mn _{0.75} Fe _{0.25} Ti-IMP	14.9	5.1	66	960
35Mn _{0.75} Fe _{0.25} Ti-IMP	26.1	8.9	71	1181
40Mn _{0.75} Fe _{0.25} Ti-IMP	29.9	10.1	63	1104
15Mn _{0.75} Fe _{0.25} Ti-DP	11.2	3.8	90	1193
25Mn _{0.75} Fe _{0.25} Ti-DP	18.7	6.3	91	1515
30Mn _{0.75} Fe _{0.25} Ti-DP	22.4	7.6	85	1401

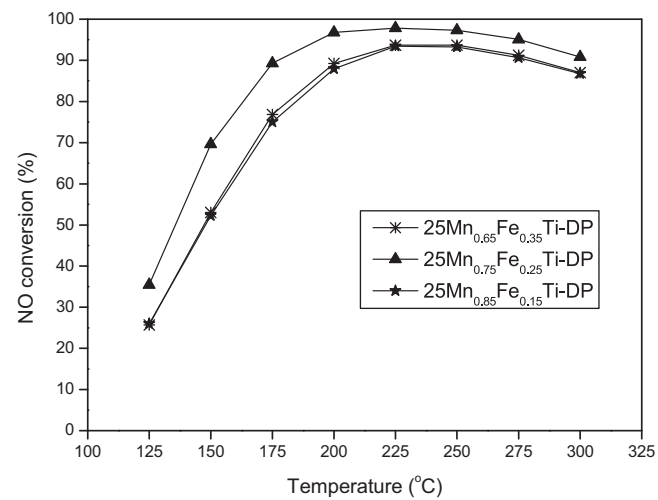


Fig. 5. Catalytic activity profiles of $25MnFeTi$ -DP catalysts with different $Mn_{0.65-0.85}-Fe_{0.35-0.15}$ mole fractions.

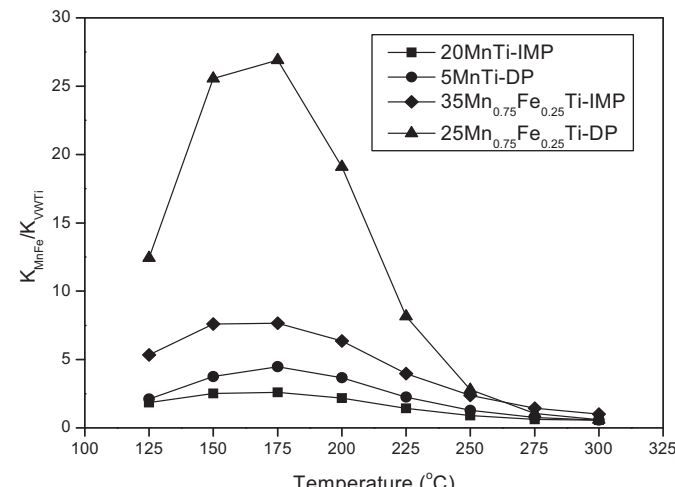


Fig. 6. Relative rate constant (k_{Mn}/k_{VWTi}) profiles of MnTi and MnFeTi catalysts.

In the present investigation, the most active $25Mn_{0.75}Fe_{0.25}Ti$ -DP catalyst displayed rate constants of 145 and $119\text{ cm}^3\text{ g}^{-1}\text{ s}^{-1}$ at dry and wet (2.3 vol.% water) conditions, respectively, at 150°C .

Physicochemical properties of Mn–Fe/TiO₂ catalysts are summarized in Table 1. The catalysts with low, optimum and high metal loadings are studied to investigate the catalyst properties. The surface area of the TiO₂ carrier was found to be $83\text{ m}^2/\text{g}$, while those of MnFeTi-IMP-loaded catalysts were lower. Especially, MnTi-IMP and MnFeTi-IMP catalysts displayed a decrease in

surface area from 60 to 42 m^2/g and 71 to 63 m^2/g , respectively by increase of metal loading. In general, the surface area of the catalyst decreases with increasing active metal loading due to pore blocking of the TiO_2 support [28]. The MnTi-DP catalysts showed almost retained surface area with increasing active metal content. Therefore, it is assumed that the manganese oxide is highly dispersed on TiO_2 support in the MnTi-DP catalysts. Surprisingly, MnFeTi-DP catalysts displayed increased surface area compared to the TiO_2 support. Wu and Qi et al. [14,16] also reported increased surface area after the addition of Fe oxide to the Mn/TiO₂ catalyst. Fig. 7 shows the cumulative surface area of the catalysts with increasing pore width. The 35Mn_{0.75}Fe_{0.25}Ti-IMP catalyst is showing less surface area compared to parent TiO_2 mainly due to loss of both microporosity and mesoporosity. Contrarily, 25Mn_{0.75}Fe_{0.25}Ti-DP catalyst showed increased microporosity compared to TiO_2 which explains the increased surface area. The increased surface area and microporosity of the 25Mn_{0.75}Fe_{0.25}Ti-DP catalyst is apparently due to contribution from manganese and iron oxide along with the TiO_2 support. This indicates that change of the method of catalyst preparation can lead to a change in surface area and porosity. Overall, low-temperature SCR activity of the 25Mn_{0.75}Fe_{0.25}Ti-DP catalyst can be related to the better surface properties and more adsorption centers as also reported by Chen et al. [29] on Fe–MnO_x catalysts prepared by the citric acid method.

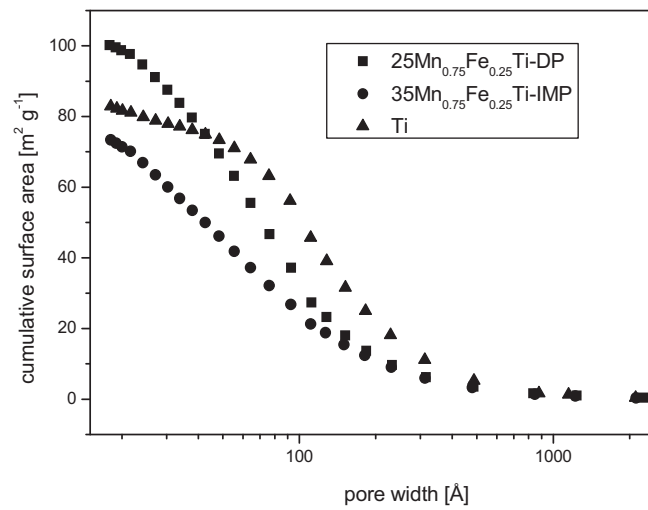


Fig. 7. Cumulative BJH surface areas as a function of the pore width.

The X-ray powder diffraction (XRPD) patterns of MnTi-IMP, MnTi-DP MnFeTi-IMP and MnFeTi-DP catalysts are shown in Fig. 8. The presence of a dominating TiO_2 support anatase phase was observed in all catalysts. The XRPD patterns of the MnTi-IMP

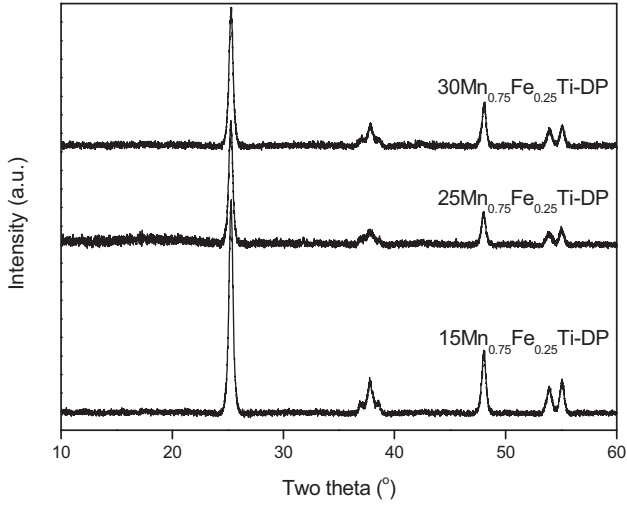
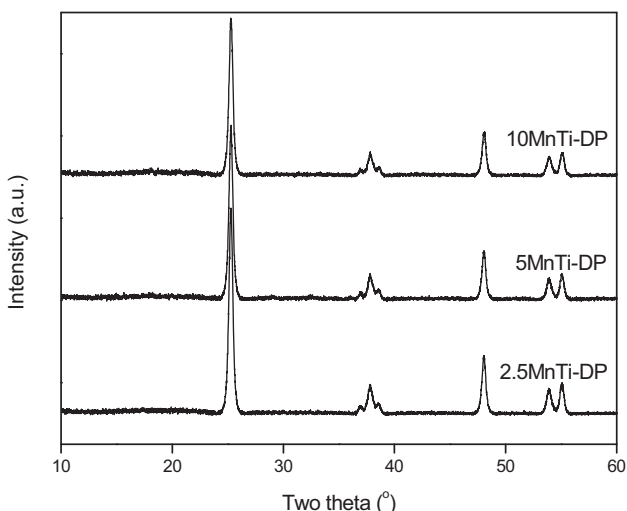
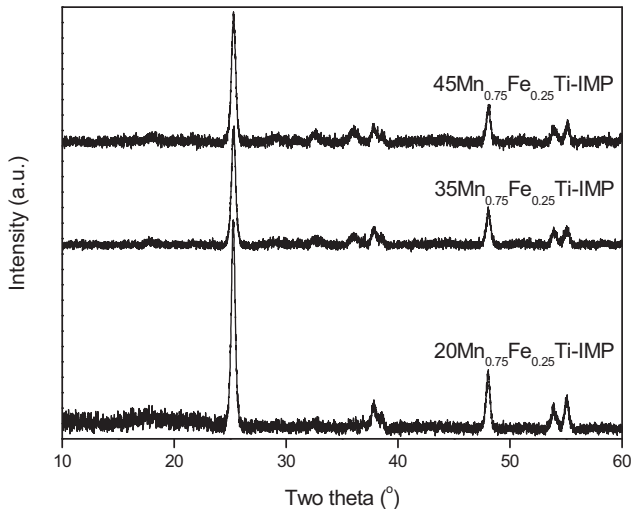
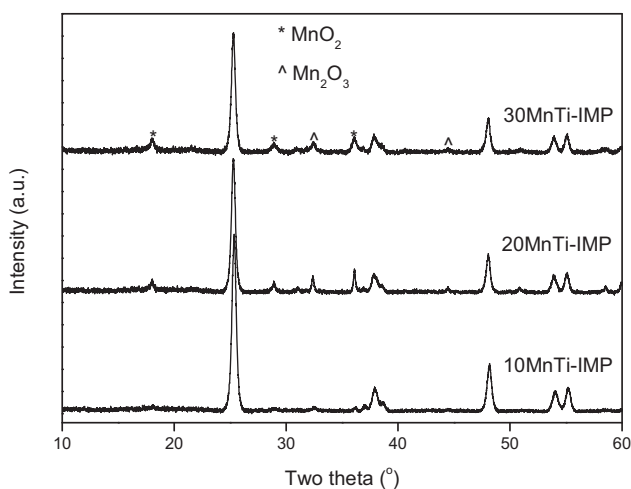


Fig. 8. XRPD patterns of MnTi-IMP, MnTi-DP, Mn_{0.75}Fe_{0.25}Ti-IMP and Mn_{0.75}Fe_{0.25}Ti-DP catalysts with different metal contents.

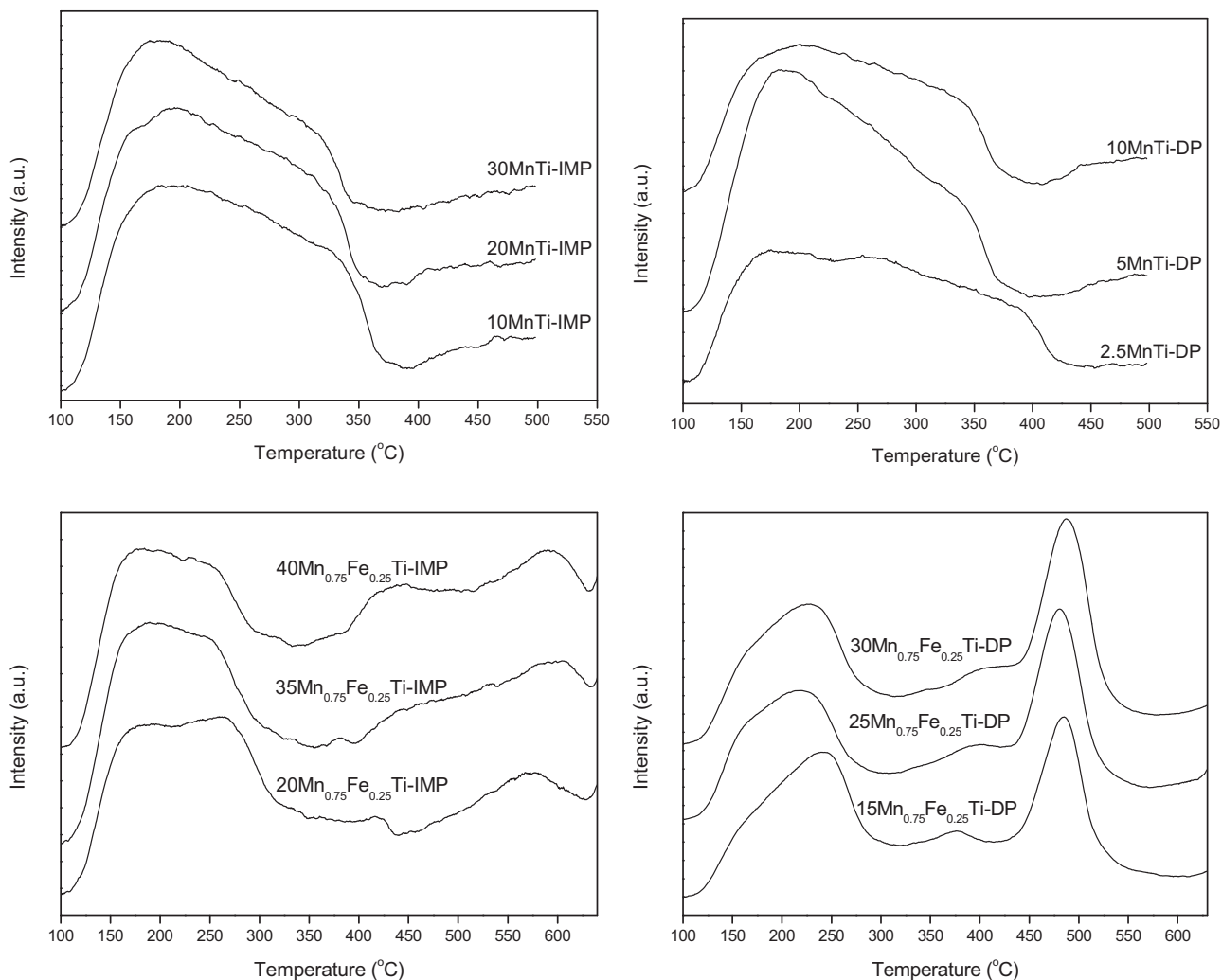


Fig. 9. NH₃-TPD profiles of MnTi-IMP, MnTi-DP, Mn_{0.75}Fe_{0.25}Ti-IMP and Mn_{0.75}Fe_{0.25}Ti-DP catalysts with different metal contents.

catalysts with different Mn loading indicate that at low loadings (i.e. at 10 wt% Mn) no manganese oxide phase can be detected. This is a clear indication that MnO_x is in a highly dispersed amorphous state at 10 wt% Mn. As the Mn loading is increased, crystalline phases of MnO_x (MnO₂ and Mn₂O₃) are observed at 20 and 30 wt% Mn loading. The calculated particle size of manganese oxide was found to be 30 nm on 20MnTi-IMP catalyst. Qi and Ettireddy et al. [16,24] reported an amorphous phase of MnO_x up to 15 wt% Mn loading in good agreement with our data. The XRPD patterns of MnTi-DP, MnFeTi-IMP and MnFeTi-DP catalysts showed only the TiO₂ support phases because of the enhanced formation of the amorphous phase of MnO_x when prepared by DP method and that dispersion of Mn is promoted by the presence of Fe. Especially, bulk manganese oxide catalysts prepared with carbonate containing precipitating agents showed amorphous structure [22]. Superior low-temperature SCR activity of amorphous transition metal oxides over the corresponding crystalline phases was reported by Kang and Tang et al. [22,23].

Temperature-programmed desorption of NH₃ (NH₃-TPD) is frequently used for determining the surface acidity of solid catalysts. The total amount of adsorbed ammonia, which is determined from the area under the TPD curve, corresponds to weakly adsorbed ammonia (temperature of desorption below 300 °C) and strongly adsorbed ammonia (temperature of desorption above 300 °C) [23,28]. The presence of acid sites is considered to favor NO conversion due to preferential adsorption of NH₃ on these sites thus

initiating the reaction [13,26]. Accordingly, one would expect a correlation of the SCR activity with the amount of total acidity (Lewis and Brönsted acidity) and acid strength (*T*_{max} of ammonia desorption).

Fig. 9 shows the NH₃-TPD desorption patterns of MnTi-IMP, MnTi-DP MnFeTi-IMP and MnFeTi-DP catalysts. The TPD profiles of MnTi-IMP and MnTi-DP catalysts exhibit only weak acid sites, whereas MnFeTi-IMP and MnFeTi-DP catalysts display both weak and strong acid sites. The NH₃-TPD results are summarized in Table 1. The total acidity of 10, 20 and 30MnTi-IMP catalysts was found to be 319, 271 and 253 μmol/g, respectively. The total acidity of 2.5, 5 and 10MnTi-DP catalysts was found to be 393, 525 and 371 μmol/g, respectively. Even with similar metal loading of 10 wt% Mn, MnTi-DP catalyst displayed moderate increase in acidity compared to IMP catalyst, probably due to the change in preparation method using ammonium carbamate as a precipitating agent leading to retained surface area. The MnFeTi-IMP and MnFeTi-DP catalysts display a marked increase in acidity compared to the MnTi catalysts, which could be due to surplus Lewis acidity in the presence of Fe [15]. Thus, the total acidity of the 35Mn_{0.75}Fe_{0.25}Ti-IMP and 25Mn_{0.75}Fe_{0.25}Ti-DP catalysts was found to be 1181 and 1515 μmol/g, respectively. As expected, the SCR activity and acidity decrease in the order 25Mn_{0.75}Fe_{0.25}Ti-DP > 35Mn_{0.75}Fe_{0.25}Ti-IMP > 5MnTi-DP > 20MnTi-IMP.

Temperature-programmed reduction with H₂ (H₂-TPR) was used to investigate the reducibility of the metal oxides. It

Table 2
H₂-TPR results of Mn–Fe/TiO₂ catalysts.

Catalyst	H ₂ consumption (μmol/g)	Average oxidation state of Mn
10MnTi-IMP	2002	2.20
20MnTi-IMP	2602	1.43
5MnTi-DP	1674	3.68
10MnTi-DP	2268	2.49
35Mn _{0.75} Fe _{0.25} Ti-IMP	4660	–
25Mn _{0.75} Fe _{0.25} Ti-DP	4120	–
5FeTi-IMP	1920	–

is known that ease of reduction of metals favors the low-temperature SCR activity [10]. The redox properties of the optimum catalysts (20MnTi-IMP, 5MnTi-DP, 35Mn_{0.75}Fe_{0.25}Ti-IMP and 25Mn_{0.75}Fe_{0.25}Ti-DP) are shown in Fig. 10. The H₂ consumption (μmol/g) and change in average oxidation state of Mn are summarized in Table 2. The 20MnTi-IMP and 5MnTi-DP catalysts show three different reduction peaks which correspond to step-wise reduction of MnO₂ to MnO as attributed in Fig. 10. The 5MnTi-DP catalyst is being reduced at comparatively lower temperatures (≈40 °C) compared to the 20MnTi-IMP catalyst. Apparently, the low-temperature reducibility of 5MnTi-DP catalyst could be due to the highly dispersed nature of manganese oxide on TiO₂ using ammonium carbonate as precipitant. The 20MnTi-IMP and 5MnTi-DP catalysts showed H₂ consumption of 2602 and 1674 μmol/g, respectively. The change in average oxidation state of Mn was calculated from the total consumption of H₂ during TPR to be 1.43 and 3.68 for 20MnTi-IMP and 5MnTi-DP, respectively. The change in average oxidation state of Mn reported in the literature [24] on 20 wt% Mn/TiO₂ catalyst prepared by impregnation was 1.68, which is close to 1.43 of the 20MnTi-IMP catalyst found in the present investigation. The change in average oxidation state of Mn is decreased with the increase in the Mn loading [24]. To see the influence of change in method of preparation, 10 MnTi catalysts are compared at similar loading. The 10MnTi-DP catalyst is being reduced at comparatively lower temperatures (≈20 °C) compared to the 10MnTi-IMP catalyst.

To distinguish the influence of Fe on Mn/TiO₂, the 5FeTi-IMP reduction pattern is also shown in Fig. 10 having a reduction temperature around 338 °C. The 35Mn_{0.75}Fe_{0.25}Ti-IMP and 25Mn_{0.75}Fe_{0.25}Ti-DP catalysts showed different reduction patterns, with only two reduction peaks. The first peak corresponds to the dominant MnO₂ reduction peak, and the second one could be due to reduction of subsequent manganese oxide phases with iron oxide. The 35Mn_{0.75}Fe_{0.25}Ti-IMP and 25Mn_{0.75}Fe_{0.25}Ti-DP catalysts display H₂ consumption of 4660 and 4120 μmol/g, respectively. Compared with the 20MnTi-IMP and 5MnTi-DP catalysts, the 35Mn_{0.75}Fe_{0.25}Ti-IMP and 25Mn_{0.75}Fe_{0.25}Ti-DP catalysts are reduced at much lower temperatures in the presence of Fe. It is evident that transition metal-doped catalysts are more easily reduced at lower temperatures than the monometallic Mn/TiO₂ catalysts [19]. Thus, low-temperature redox properties and dominant MnO₂ phase in MnFeTi catalysts are the main contributors to the superior low-temperature SCR activity. Overall, the redox patterns of these optimum catalysts are not identical due to change in method of preparation, Mn loading and bimetallic influence of Fe.

The XPS spectra for Ti 2p, Mn 2p, Fe 2p and O 1s of (a) 35Mn_{0.75}Fe_{0.25}Ti-IMP and (b) 25Mn_{0.75}Fe_{0.25}Ti-DP catalysts and BE

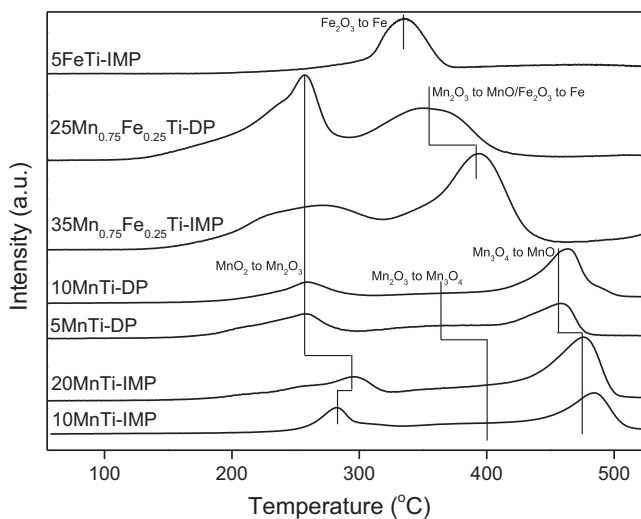


Fig. 10. H₂-TPR profiles of 10MnTi-IMP, 20MnTi-IMP, 5MnTi-DP, 10MnTi-DP, 35Mn_{0.75}Fe_{0.25}Ti-IMP, 25Mn_{0.75}Fe_{0.25}Ti-DP and 5FeTi-IMP catalysts.

(eV) values are reported in the supplement. Two main peaks due to Ti 2p_{3/2} and Ti 2p_{1/2} were positioned at 458 and 464 eV, respectively. Two main peaks due to Mn 2p_{3/2} and Mn 2p_{1/2} were observed at 642 and 653 eV, respectively. The characteristic peak of Fe 2p_{3/2} and Fe 2p_{1/2} were observed at 711 and 724 eV, respectively. The XPS spectra of O 1s are shown with two deconvoluted peaks, a major one at about 530 eV and a minor one at about 532 eV. The former peak (O_β) can be assigned to lattice oxygen and the latter peak (O_α) to chemisorbed surface oxygen. The distribution of the elements on the surface obtained by XPS characterization is shown in Table 3. Optimum 25Mn_{0.75}Fe_{0.25}Ti-DP and 35Mn_{0.75}Fe_{0.25}Ti-IMP catalysts showed a surface atom Mn/Fe ratio of 2.72 and 2.02, respectively. Thus, we can assume that the change in the method of preparation resulted in an active MnFe oxide species on the surface of the support. It is important to notice that 25Mn_{0.75}Fe_{0.25}Ti-DP yields an O_α concentration of 50.1% of the total oxygen, while the 35Mn_{0.75}Fe_{0.25}Ti-IMP catalyst only yields 31.3%. The beneficial influence of high concentrations of chemisorbed oxygen on the low-temperature SCR reaction has been reported before [14,29–31] and is explained by an increased rate of NO to NO₂ oxidation [31]. Furthermore, the Mn/Fe ratio is lower in 25Mn_{0.75}Fe_{0.25}Ti-DP than in 35Mn_{0.75}Fe_{0.25}Ti-IMP. In other words, the DP method leads to a higher relative surface concentration of Fe on the surface of the catalyst. A reaction mechanism of the reduction of NO by NH₃ over MnO_x has been proposed by Kapteijn et al. [25]. The NH₃ adsorbs onto the surface where it is dehydrogenated to give surface adsorbed NH₂. The dehydrogenation is favored by high levels of reactive surface oxygen (O_α). The surface-adsorbed NH₂ can further react with NO to yield N₂ and H₂O via surface-adsorbed NH₂NO [32]. Our XPS results have shown that the DP-prepared catalyst contains significantly more reactive surface oxygen (O_α) than the IMP-prepared one.

The favorable influence of a high rate of NO to NO₂ oxidation was reported several times before [16,29]. Fig. 11 shows the oxidation of NO to NO₂ on 35Mn_{0.75}Fe_{0.25}Ti-IMP and 25Mn_{0.75}Fe_{0.25}Ti-DP catalysts at 150 °C under dry and wet conditions. 35Mn_{0.75}Fe_{0.25}Ti-IMP

Table 3
Atomic % of 35Mn_{0.75}Fe_{0.25}Ti-IMP and 25Mn_{0.75}Fe_{0.25}Ti-DP catalysts determined by XPS.

Catalyst	Ti	Mn	Fe	Mn/Fe	O _t	O _α /O _t
35Mn _{0.75} Fe _{0.25} Ti-IMP	12.0	16.7	6.7	2.72	64.6	31.3
25Mn _{0.75} Fe _{0.25} Ti-DP	14.5	8.8	4.1	2.08	72.6	50.1

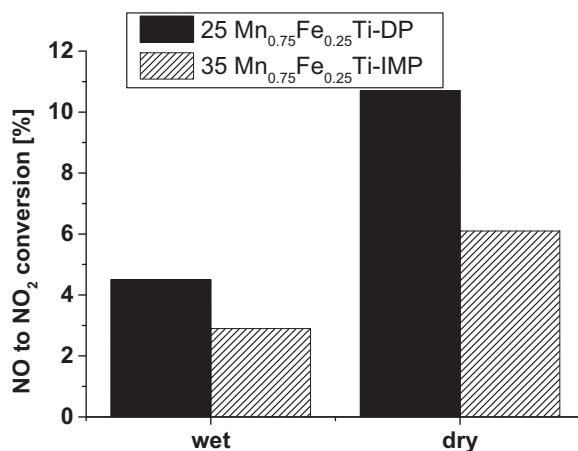


Fig. 11. Oxidation of NO to NO₂ on 35Mn_{0.75}Fe_{0.25}Ti-IMP and 25Mn_{0.75}Fe_{0.25}Ti-DP catalysts. Reaction conditions: [NO] = 1000 ppm, [O₂] = 4%, [H₂O] = 0 or 2%, w_{cat} = 0.1 g (180–300 μ m), F = 150 mL min⁻¹, T = 150 °C.

and 25Mn_{0.75}Fe_{0.25}Ti-DP catalysts showed NO to NO₂ conversion of 6 and 10.5% under dry conditions, respectively. Under wet conditions, the 35Mn_{0.75}Fe_{0.25}Ti-IMP and 25Mn_{0.75}Fe_{0.25}Ti-DP catalysts displayed NO to NO₂ conversion of 3 and 4.5%, respectively.

The TGA profiles of 35Mn_{0.75}Fe_{0.25}Ti-IMP and 25Mn_{0.75}Fe_{0.25}Ti-DP catalysts are reported in the supplement. The 35Mn_{0.75}Fe_{0.25}Ti-IMP catalyst shows continuous weight loss up to 600 °C with a total weight loss of about 3 wt%, while the 25Mn_{0.75}Fe_{0.25}Ti-DP catalyst loses more than 5 wt% and exhibits two steps at around 425 and 525 °C. A possible explanation for the higher weight loss of 25Mn_{0.75}Fe_{0.25}Ti-DP catalyst is its higher content of chemisorbed oxygen as determined by XPS.

4. Conclusions

A range of MnTi and MnFeTi catalysts prepared by both impregnation and by deposition-precipitation (DP) methods are highly active for low-temperature SCR of NO with NH₃. Additionally, the DP method of preparation decreases the metal loading (25 wt%) required to reach the optimum activity compared to the IMP method (35 wt%). The relative activity of the most active 25Mn_{0.75}Fe_{0.25}Ti-DP catalyst is 26.9 times higher than a standard industrial-type VWTi catalyst at 175 °C. The 25Mn_{0.75}Fe_{0.25}Ti-DP catalyst displayed unique and optimum catalyst properties with respect to high surface area, acidity, redox properties and high content of chemisorbed oxygen.

Acknowledgements

This work was financially supported by Energinet.dk through the PSO project 10521. LAB S.A., France, and DONG Energy, Denmark, are also thanked for financial support and valuable discussions.

Appendix A. Supplementary data

Supplementary data associated with this article can be found, in the online version, at <http://dx.doi.org/10.1016/j.apcatb.2014.10.060>.

References

- [1] H. Bosch, F.J.G. Janssen, *Catal. Today* 2 (1988) 369.
- [2] G. Busca, L. Lietti, G. Ramis, F. Berti, *Appl. Catal. B* 18 (1998) 1.
- [3] V.I. Parvulescu, P. Grange, B. Delmon, *Catal. Today* 46 (1998) 233.
- [4] J. Ando, *Flue Gas Cleaning Technology of the World*, Coal Mining Research Institute, Tokyo, Japan, 1990, 326 pp.
- [5] Z. Huang, X. Gu, W. Wen, P. Hu, M. Makkee, H. Lin, F. Kapteijn, X. Tang, *Angew. Chem. Int. Ed.* 52 (2013) 660.
- [6] Z. Liu, Y. Yi, S. Zhang, T. Zhu, J. Zhu, J. Wang, *Catal. Today* 216 (2013) 76.
- [7] L. Singoredjo, R. Korver, F. Kapteijn, J. Moulijn, *Appl. Catal. B* 1 (1992) 297.
- [8] P.G. Smirniotis, D.A. Peña, B.S. Uphade, *Angew. Chem. Int. Ed.* 40 (2001) 2479.
- [9] S. Roy, M.S. Hegde, G. Madras, *Appl. Energy* 86 (2009) 2283.
- [10] A. Sultana, M. Sasaki, H. Hamada, *Catal. Today* 185 (2012) 284.
- [11] R.Q. Long, R.T. Yang, R. Chang, *Chem. Commun.* (2002) 452.
- [12] Y. Kim, H.J. Kwon, I. Nam, J.W. Choung, J.K. Kil, H. Kim, M. Cha, G.K. Yeo, *Catal. Today* 151 (2010) 244.
- [13] J. Li, H. Chang, L. Ma, J. Hao, R.T. Yang, *Catal. Today* 175 (2011) 147.
- [14] Z. Wu, B. Jiang, Y. Liu, *Appl. Catal. B* 79 (2008) 347.
- [15] S. Roy, B. Viswanath, M.S. Hegde, G. Madras, *J. Phys. Chem. C* 112 (2008) 6002.
- [16] G. Qi, R.T. Yang, *Appl. Catal. B* 44 (2003) 217.
- [17] G. Qi, R.T. Yang, R. Chang, *Appl. Catal. B* 51 (2004) 93.
- [18] D.A. Peña, B.S. Uphade, P.G. Smirniotis, *J. Catal.* 221 (2004) 421.
- [19] B. Thirupathi, P.G. Smirniotis, *J. Catal.* 288 (2012) 74.
- [20] B. Jiang, Y. Liu, Z. Wu, J. Hazard. Mater. 145 (2007) 488.
- [21] J. Li, J. Chen, R. Ke, C. Luo, J. Hao, *Catal. Commun.* 8 (2007) 1896.
- [22] M. Kang, E.D. Park, J.M. Kim, J.E. Ye, *Appl. Catal. A* 327 (2007) 261.
- [23] X. Tang, J. Hao, W. Xu, J. Li, *Catal. Commun.* 8 (2007) 329.
- [24] P.R. Ettireddy, N. Ettireddy, S. Mamedov, P. Boolchand, P.G. Smirniotis, *Appl. Catal. B* 76 (2007) 123.
- [25] F. Kapteijn, L. Singoredjo, A. Andreini, J.A. Moulijn, *Appl. Catal. B* 3 (1994) 173.
- [26] S. Yang, C. Wang, J. Li, N. Yan, L. Ma, H. Chang, *Appl. Catal. B* 110 (2011) 71.
- [27] F. Kapteijn, L. Singoredjo, N.J.J. Dekker, J.A. Moulijn, *Ind. Eng. Chem. Res.* 32 (1993) 445–452.
- [28] S.S.R. Putluru, A.D. Jensen, A. Riisager, R. Fehrmann, *Catal. Sci. Technol.* 1 (2011) 631.
- [29] Z. Chen, F. Wang, H. Li, Q. Yang, L. Wang, X. Li, *Ind. Eng. Chem. Res.* 51 (2012) 202.
- [30] S. Boxiong, Y. Yan, H. Hongqing, L. Ting, *Chin. J. Catal.* 32 (2011) 1803.
- [31] B. Shen, T. Liu, N. Zhao, X. Yang, L. Deng, *J. Environ. Sci.* 22 (2010) 1447.
- [32] Z. Wu, B. Jiang, Y. Liu, H. Wang, R. Jin, *Environ. Sci. Technol.* 41 (2007) 5812.